Phys Chem Minerals (2004) 31: 122–129
DOI 10.1007/s00269-004-0380-4
© Springer-Verlag 2004

ORIGINAL PAPER

D. Levy · V. Diella · M. Dapiaggi · A. Sani
M. Gemmi · A. Pavese

Equation of state, structural behaviour and phase diagram of synthetic $MgFe_2O_4$, as a function of pressure and temperature

Received: 11 August 2003 / Accepted: 15 November 2003

Abstract The behaviour of synthetic Mg-ferrite ($MgFe_2O_4$) has been investigated at high pressure (in situ high-pressure synchrotron radiation powder diffraction at ESRF) and at high temperature (in situ high-temperature X-ray powder diffraction) conditions. The elastic properties determined by the third-order Birch–Murnaghan equation of state result in $K_0 = 181.5(\pm\ 1.3)$ GPa, $K' = 6.32(\pm\ 0.14)$ and $K'' = -0.0638$ GPa^{-1}. The symmetry-independent coordinate of oxygen does not show significant sensitivity to pressure, and the structure shrinking is mainly attributable to the shortening of the cell edge (homogeneous strain). The lattice parameter thermal expansion is described by $\alpha_{a0} + \alpha_{a1}{}^*(T-298) + \alpha_{a2}/(T-298)^2$, where $\alpha_{a0} = 9.1(1)\ 10^{-6}$ K^{-1}, $\alpha_{a1} = 4.9(2)\ \ 10^{-9}$ K^{-2} and $\alpha_{a2} = \ \ 5.1(5)\ 10^{-2}$ K. The high-temperature cation-ordering reaction which MgFe-spinel undergoes has been interpreted by the O'Neill model, whose parameters are $\alpha = 22.2(\pm\ 1.8)$ kJ mol^{-1} and $\beta = -17.6(\pm\ 1.2)$ kJ mol^{-1}. The elastic and thermal properties measured have then been used to model the phase diagram of $MgFe_2O_4$, which shows that the high-pressure transition from spinel to orthorombic $CaMn_2O_4$-like structure at $T < 1700$ K is preceded by a decomposition into MgO and Fe_2O_3.

Keywords $MgFe_2O_4$ · Behaviour as a function of P and T · Phase diagram

D. Levy
Dipartimento Scienze Mineralogiche e Petrologiche-Università degli Studi di Torino, Via Valperga Caluso 35, 10025 Torino, Italy

V. Diella · A. Pavese (✉)
National Research Council, IDPA, Section of Milan, Via Botticelli 23, 20133 Milano, Italy
Tel.: +39 02 503 15603
Fax: +39 02 503 15597
e-mail: alessandro.pavese@unimi.it

M. Dapiaggi · M. Gemmi
Dipartimento Scienze della Terra, Università degli Studi di Milano, Via Botticelli 23, 20133 Milano, Italy

A. Sani
European Synchrotron Radiation Facility, ESRF, F 38043 Grenoble Cedex, France

Present address: A. Pavese
Dipartimento Scienze della Terra, Università degli Studi di Milano
Via Botticelli 23, 20133 Milano, Italy

Introduction

The behaviour of spinels under non-ambient conditions [high pressure (HP), high temperature (HT), high pressure and temperature (HPHT)] has been subject of several studies, in terms of equilibrium properties and phase transformations. It is well known that spinels undergo a T-activated cation order–disorder transition, which involves atomic exchange between tetrahedral and octahedral sites (see Redfern 2002 for a review) and may be used to infer the thermal path experienced by a sample (Sack 1982). Moreover, the spinel structure and its $CaMn_2O_4$-, $CaFe_2O_4$- and $CaTiO_4$-like modifications (Finger et al. 1986; Pavese et al. 1999; Levy et al. 2003) play an important role in modelling major mineral phases of the mantle of the Earth (Kesson et al. 1994; Navrotsky 1994). Such transformations at high pressure are allowed by the empty tetrahedral site in the spinel structure, which gives room for structural readjustments upon increasing P (Liu 1978; Irifune et al. 1991; Funamori et al. 1998; Akaogi et al. 1999; Fei et al. 1999; Levy et al. 2000; Andrault and Bolfan–Casanova 2001).

In this view, the knowledge of the behaviour of spinels under non-ambient conditions is useful to understand the general properties of a structure model important to investigate a variety of petrologic reactions at HT and HPHT, as stated above. We focus on magnesioferrite, i.e. $MgFe_2O_4$, which ideally has an inverse structure, meaning that Mg and half Fe atoms occupy the octahedral sites (M), whereas the remaining

Fe atoms distribute over the tetrahedral sites (T). The behaviour of this spinel as a function of P was earlier studied by Andrault and Bolfan–Casanova (2001), using HP powder diffraction, and then by Wang et al. (2002), by means of HP Raman spectroscopy. Order–disorder reactions in $MgFe_2O_4$ spinel triggered by heating were investigated by O'Neill et al. (1992), using quenched synthetic samples.

The aim of the present work is twofold: (1) to contribute to the completion of the systematic study on the properties of the spinel group under non-ambient conditions as a function of composition (see the references quoted above) by investigating the structural and elastic properties of $MgFe_2O_4$ by means of in situ high-pressure (ID9 A beamline at ESRF) and in situ high-temperature (laboratory Brentano geometry diffractometer) powder diffraction; (2) to contribute to understand the P–T phase diagram of $MgFe_2O_4$, exploiting the results obtained at point (1) (in particular the elastic properties and thermal expansion) in equilibrium thermodynamic calculations.

Experimental

Sample

The Mg-ferrite sample was synthesised by mixing analytical purity MgO and Fe_2O_3 reagent grades (Carlo Erba Reagenti), the former in slight excess as suggested by O'Neill et al. (1992). The sample was heated up to 1000 °C for 3 days, then brought first to 950 °C for 1 day, successively to 900 °C for 1 day more, and finally cooled down at an estimated rate of ≈20–25 °C h^{-1} to ambient temperature. The excess of magnesium oxide was removed by washing the powder by dilute nitric acid. A powder diffraction pattern collected with a laboratory diffractometer (X'Pert Philips) did not reveal occurrence of any parent phase. Chemical analyses were performed using an Applied Research Laboratories SEMQ microprobe equipped with six wavelength-dispersive crystals. Natural kaersutite was used as a standard for Mg and Fe contents. The chemical composition of the synthesised spinel was determined by averaging ten analyses performed on a polished epoxy cemented powder and resulted in $MgO = 20.5 \pm 0.6$ and $Fe_2O_3 = 79.7 \pm 0.6$ wt%, corresponding to a formula unit as $Mg_{1.02(2)}Fe_{1.99(1)}O_4$. The uncertainties shown take into account the propagation of errors in averaging. Hereafter we assume the ideal composition $MgFe_2O_4$; this approximation is consistent with the uncertainties observed. The structure parameters were obtained by a Rietveld refinement, which gave $a = 8.39389(5)$ Å, $u = 0.2563(1)$ [(u,u,u) position of oxygen] and $x = 0.802(11)$ (Fe occupancy at the T-site).

Powder diffraction under HP conditions

The high-pressure powder diffraction measurements were carried out at ESRF (Grenoble, F) on ID9 A beamline, using an angle disperse setup. High pressure was achieved by two diamond anvil cells (DAC) equipped with 600-μm and 250-μm culets to explore the pressure ranges 0–8 GPa (silicon oil as a pressure-transmitting medium) and 2–43 GPa (nitrogen as a pressure-transmitting medium), respectively. We used data from the first run below 2 GPa, where the environment is still hydrostatic, and from the second one at higher pressures; data above 35 GPa are not contemplated in the present analysis, which relies upon 28 HP diffraction patterns, because the sample began to transform into a new phase. Pressure was determined by the shift of the fluorescence line of a ruby excited by an Ar laser, and using the non-linear hydrostatic pressure scale of Mao et al. (1986). The ruby crystal was placed in the HP cell so as to be in the centre of the incident X-ray beam; a second ruby was positioned close to the rim of the gasket, to estimate the pressure gradient, but, unfortunately, it proved of too low a quality for a precise determination of pressure. Equilibrium was assumed achieved when pressure, measured every 10th min, did not oscillate more than 0.01 GPa. The uncertainties on P were estimated about 0.1 GPa on the basis of earlier measurements under the same conditions. No correction was used to account for deviations from hydrostaticity; note, however, that (1) Levy et al. (2003) observed, using the same experimental setup and a spinel sample, that the results attained correcting the experimental pressures by a linear model are in agreement with those determined using raw P values; (2) following the approach of Singh (1993) and Duffy et al. (1995), and using the 220 and 311 diffraction peaks, we calculated a difference between the stress components along the thrust axis and normal to it of ≈0.17 GPa, consistently with an average uncertainty on P of 0.1 GPa. Owing to point (2), one expects to have χ^2 values from the EoS fits larger than unity.

The X-ray beam from an U46 undulator was focalised vertically by a Pt-coated silicon mirror and horizontally by an asymmetrically cut bent Si(111) Laue monochromator to a spot size of about 30×30 μm^2. Diffraction images were collected by a MAR345 imaging plate (pixel size 100×100 μm^2) with a wavelength of $\lambda = 0.41507$ Å, calibrated with Si-NBS. Such a detector (sample to plate distance of 359.935 mm) provides an angular resolution of about 0.04° and allows a data collection time smaller than 30 s. The two-dimensional images of the diffraction rings were integrated into 2ϑ patterns using the FIT2D software package (Hammersley et al. 1996). The diffraction profiles were treated by means of the EXPGUI-GSAS codes (Larson and Von Dreele 2000; Toby 2001) to perform Rietveld structure refinements. The pseudo-Voigt profile function proved to be appropriate to treat our diffraction patterns; the Gaussian and Lorentzian contributions to the FWHM were parameterised as $\sigma^2 = \sigma_0 \tan(\vartheta)^2$ and $\gamma = \gamma_0/\cos(\vartheta)$(if $P < 10$ GPa) or $\gamma = \gamma_0 \tan(\vartheta)$ (if $P > 10$ GPa). The background was modelled by a shifted Chebyschev polynomial function with 15 coefficients. The contribution of the crystalline N_2 was first treated by a multiphase refinement. This approach proved scarcely efficient, and we chose to manually erase the contribution of the crystalline N_2 at the image integration stage. However, the overlap between the peaks of the spinel phase and N_2 made it impossible to eliminate the nitrogen contributions in the pressure range between 19 and 35 GPa.

The quality of the collected powder patterns allowed full structural refinements: the cell parameter, atomic position, tetrahedral and octahedral site occupancy factors were determined as a function of pressure up to ≈35 GPa.

Powder diffraction under HT conditions

High-temperature X-ray powder diffraction was performed on a laboratory diffractometer (Philips X'Pert), equipped with a high-temperature chamber (AHT PAP-1600) that enables an optimal sample position over the whole temperature range, by means of a stepper motor which moves the sample downwards as a function of the sample holder's thermal expansion. In this way, it is possible to obtain good-quality data even at the highest achievable temperature (about 1900 K). Si-NBS was used as an inner calibrant, and allowed one to fix the spinel cell and the goniometer zero. Data collections were carried out every 100th K, up to 1473 K, between 17 and 118° 2ϑ, with a step size of 0.02° 2ϑ, a counting time of 4 s per step, and using a heating rate of 25° min^{-1}. Before any HT data collection, temperature was kept fixed for 2 h to achieve thermal equilibrium. The actual temperature was determined by a calibration (Dapiaggi et al. 2002) regularly checked by standard silicon thermal expansion (Swenson 1993); the uncertainty in temperature can be estimated about ±2 K. The structure refinements were performed by the GSAS-EXPGUI packages (Toby 2001; Larson and Von Dreele 2000). The pseudo-Voigt profile function proved to

be appropriate to treat the high-temperature diffraction patterns; the FWHMs of the Gaussian and Lorentzian components were parameterised as $\sigma^2 = C$ (where C is a constant) and $\gamma = \gamma_0/\cos(\vartheta)$, respectively. The goniometer zero determined at room temperature was kept fixed in the high-temperature structure refinements (a total of 17 patterns).

Theoretical

Equations of state

The bulk elastic properties of spinel were investigated by fitting the Birch–Murnaghan EoS (Birch 1986), the Vinet EoS (Vinet et al. 1986, 1987) and the Poirier–Tarantola EoS (Poirier and Tarantola 1998) to the measured pressure values.

The Birch-Murnaghan model results in:

$$P(V) = 3K_0 f_E(1+2f_E)^{5/2}\left(1 + Af_E + Bf_E^2\right) \ , \qquad (1)$$

where K_0 is the bulk modulus at $P = 0.00001$ GPa (hereafter indicated as $P = 0$, for the sake of brevity), $A = 3/2(K'-4)$ and $B = 3/2[K_0K'' + (K'-4)(K'-3) + 35/9]$, with K' and K'' corresponding to the first and second derivative of K versus P, at $P = 0$; f_E is the Eulerian strain defined as follows:

$$f_E = \left[(V_0/V)^{2/3} - 1\right]/2 \ , \qquad (2)$$

where V_0 and V stand for the volume at $P = 0$ and at a given pressure, respectively.

The Vinet EoS is expressed as:

$$P(V) = 3K_0 \frac{(1-f_V)}{f_V^2}\exp[\eta(1-f_V)] \ , \qquad (3)$$

where $\eta = 3/2(K'-1)$ and $f_V = (V/V_0)^{1/3}$.

The Poirier–Tarantola EoS calculates pressure as:

$$P(V) = 3K_0\left(\frac{V_0}{V}\right)f_N\left(1 + Af_N + Bf_N^2\right) \ , \qquad (4)$$

where $A = 3/2(K'-2)$, $B = 3/2[1 + K_0K'' + (K'-2) + (K'-2)^2]$ and f_N is defined as $f_N = 1/3\ \ln(V_0/V)$.

Equilibrium thermodynamic calculations

The stability of a given phase or assemblage at (P_2,T_2) has been determined via its Gibbs energy, which is calculated (1) assuming a known reference pressure-temperature [($P_{\rm ref}$, $T_{\rm ref}$), generally room conditions] the formation enthalpy from elemental constituents ($H^f_{\rm ref}$), and (2) integrating $C_p{\rm d}T$ and $V{\rm d}P$ along the isobaric ($P_{\rm ref}$, $T_{\rm ref}$)–($P_{\rm ref}$, T_2) and the isotherm ($P_{\rm ref}$, T_2)–(P_2,T_2), respectively. In so doing one obtains:

$$G(P_2,T_2) = H^f_{\rm ref} + \int_{\rm ref}^{1} C_p{\rm d}T - T_2\int_{\rm ref}^{1} C_p/T{\rm d}T - T_2S_{\rm ref} + \int_{2}^{1} V{\rm d}P \ ,$$

where ref, 1 and 2 stand for ($P_{\rm ref}$, $T_{\rm ref}$), ($P_{\rm ref}$, T_2) and (P_2, T_2); C_p is the specific heat at constant pressure and S the entropy.

The location of the reactions was determined by the PeRpLeX algorithm (Connolly 1990), assuming the high-pressure phase of $MgFe_2O_4$ to have the same C_p and ${\rm d}K/{\rm d}T$ of spinel, because of want of original data. Other assumptions are detailed in the Phase relation diagram calculations section below. The equilibrium volume at given P and T was computed by using the Murnaghan EoS, which allows one to express V as a function of P and T and simplifies calculations; note, however, that such an EoS is appropriate for pressures lower than ours. The approximations mentioned introduce a degree of imprecision in locating the reactions borders, and therefore one has to take care in assessing the theoretical phase diagram here presented.

Results and discussion

Bulk elastic parameters

In Figure 1 the powder diffraction pattern at ≈17 GPa is shown. The lattice parameter [a] and coordinate [u] of oxygen are given in Table 1 as a function of pressure (note that the uncertainties on lattice parameters determined from Rietveld treatment are usually affected by underestimation); a versus P is displayed in Fig. 2. Table 2 reports the elastic parameters determined using the EoS models mentioned above; v means that V_0 has been refined. The refined V_0 does not shift more than 1.5σ from its experimental value. Although the refinement of V_0 leads to a decrease of χ^2, we are inclined to attribute this improvement to V_0 behaving as a "fictitious" degree of freedom, which contributes to minimise the disagreement between measured and calculated pressures (see Pavese 2002). Such an interpretation

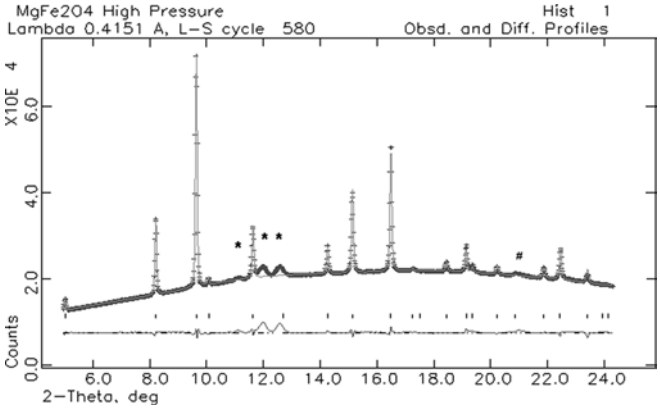

Fig. 1 Experimental (*crosses*) and calculated (*full line* by Rietveld fit) powder diffraction patterns of synthetic spinel at 17 GPa; the residual curve and peak position markers are shown. *Stars* and *dieses* indicates the peak positions of crystalline N_2 and the contribution due to the gasket, respectively

Table 1 Results from structure Rietveld refinements under high-pressure conditions: lattice parameter (Å) and u coordinate of oxygen for spinel. R_{wp} = sqrt[$\Sigma(I_o-I_c)^2 w$], where w = weighting factor

P(GPa)	a(Å)	u	R_{wp}
0.0	8.39389(5)	0.2563(1)	1.14
0.11(0.1)	8.39230(5)	0.2564(1)	1.41
0.48(0.1)	8.38596(6)	0.2562(1)	1.44
1.21(0.1)	8.37649(9)	0.2564(2)	1.41
1.81(0.1)	8.3676(1)	0.2562(2)	1.41
2.48(0.1)	8.3586(2)	0.2565(2)	3.80
3.06(0.1)	8.3540(2)	0.2564(2)	4.62
3.38(0.1)	8.3466(2)	0.2568(2)	5.23
4.28(0.1)	8.3324(1)	0.2561(2)	5.12
5.02(0.1)	8.32381(9)	0.2554(2)	5.03
6.10(0.1)	8.31178(6)	0.2560(2)	1.30
7.15(0.1)	8.29759(7)	0.2564(2)	1.67
8.14(0.1)	8.28469(8)	0.2561(2)	2.37
8.94(0.1)	8.27321(8)	0.2561(2)	2.14
10.35(0.1)	8.25608(9)	0.2555(3)	2.46
11.12(0.1)	8.2477(1)	0.2553(5)	1.17
12.07(0.1)	8.2409(1)	0.2561(4)	1.13
13.59(0.1)	8.2218(1)	0.2573(2)	0.88
17.09(0.1)	8.1885(1)	0.2566(2)	0.91
18.80(0.1)	8.1693(1)	0.2562(2)	0.84
19.48(0.1)	8.1659(1)	0.2570(2)	0.95
20.00(0.1)	8.1611(1)	0.2563(2)	0.94
20.70(0.1)	8.1532(1)	0.2563(2)	0.98
24.13(0.1)	8.1236(2)	0.2567(3)	1.17
25.54(0.1)	8.1143(3)	0.2559(4)	1.40
27.53(0.1)	8.0961(4)	0.2568(4)	2.23
29.58(0.1)	8.0815(4)	0.2568(4)	2.27
32.18(0.1)	8.0598(4)	0.2570(3)	1.23
34.39(0.1)	8.0467(4)	0.2568(3)	1.17

agrees with the observation that the P errors are probably underestimated, as hinted by the χ^2 values significantly above unity and in keeping with neglecting the deviation from non-hydrostaticity, as discussed in the Powder diffraction under HP conditions section above. Therefore, we restrict our analysis to the elastic parameters derived with V_0 fixed at its experimental value. BM4 and PT4 give smaller χ^2s than the corresponding third-order models, but yield a significant increase of the uncertainties on the elastic parameters and

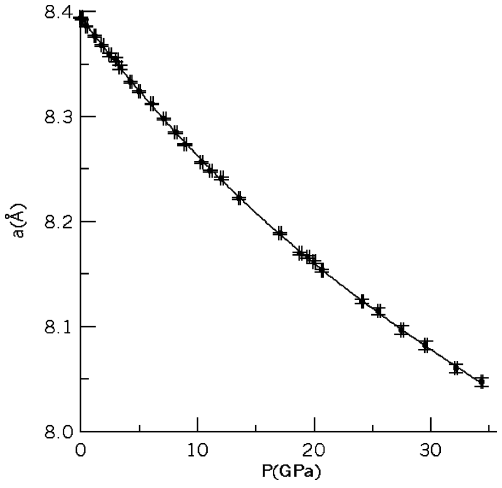

Fig. 2 Cell edge (Å) as a function of pressure (GPa). The *solid line* is the third-order polynomial fit

provide a K'' value less significant than 3σ. This is consistent with Fig. 3a and b, which displays a linear trend of the normalised pressure as a function of the strain [f_E and f_N]. In such a view, we choose to focus our attention on the issues of those models involving K_0 and K' only. Our selection can be facilitated by considering that PT3 yields significantly larger χ^2, whereas BM3 and V provide results fully comparable with each other. The bulk modulus by Andrault and Bolfan–Casanova (2001), who report a K_0 as large as 195(± 17) GPa, is consistent within the reported uncertainty with ours. Note that the higher K_0 value obtained by the quoted authors may be related to the fact they set K' at 4.

Above 35 GPa we observed the sample to undergo a transformation, first suggested by an undue broadening of the diffraction peaks, and then by the appearance of a new diffraction pattern. We did not explore whether this is a stable or metastable phase, which often occurs under HP conditions without heating, because the quality of the diffraction patterns was not such as to allow an unambiguous determination of the product of the transformation.

Table 2 K_0, K' and K'' are the bulk modulus, its first and second derivatives versus pressure, respectively, under room conditions, according to the Birch–Murnaghan, the Vinet and Poirier–Tarantola EoS. V_0 is the cell volume at room conditions. K_0'' reported without uncertainties means the value attained setting $B = 0$ in Eqs. (1) and (4). *BM3* = third-order Birch–Murnaghan EoS; *BM3v* third-order Bich–Murnaghan EoS with refined V_0; *V* Vinet model; *Vv* Vinet model with refined V_0; *PT3* third-order-Poirier–Tarantola EoS; *PT3v* third-order Poirier–Tarantola EoS with refined V_0. χ^2 = sqrt[$\Sigma(P_{obs}-P_{calc})^2/\sigma_t^2$]/($N$–$M$), where N = number of pressure measurements, M degrees of freedom; σ_t = sqrt[$\sigma(P)^2 + (\partial P/\partial V)^2\sigma(V)^2$]

EoS model	K_0(GPa)	K_0'	K_0''(GPa^{-1})	V_0(Å^3)	χ2
BM3	181.5(± 1.3)	6.32(± 0.14)	–0.0638	591.4116	2.1
BM3v	177.7(± 2.4)	6.59(± 0.19)	–0.0743	591.76(± 0.20)	1.9
BM4	187.4(± 2.9)	4.68(± 0.73)	0.11(± 0.06)	591.4116	1.8
BM4v	184.0(± 5.3)	5.20(± 1.00)	0.07(± 0.08)	591.58(± 0.22)	1.8
V	181.2(± 1.3)	6.39(± 0.14)	–	591.4116	2.1
Vv	177.4(± 2.3)	6.64(± 0.19)	–	591.77(± 0.19)	1.9
PT3	178.7(± 1.6)	7.15(± 0.18)	–0.1826	591.4116	2.4
PT3v	173.5(± 2.9)	7.64(± 0.25)	–0.2218	591.87(± 0.21)	2.1
PT4	188.3(± 3.2)	4.27(± 0.82)	0.20(± 0.08)	591.4116	1.8
PT4v	185.3(± 5.6)	4.78(± 1.10)	0.15(± 0.10)	591.56(± 0.22)	1.8

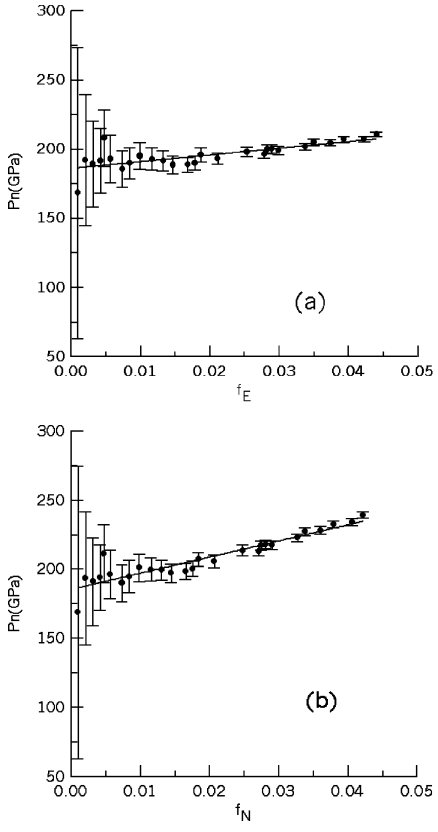

Fig. 3 Normalised pressure (GPa) versus strain, according to the Birch–Murnaghan (**a**), $P_n = P/[3\,f_E\,(1+2\,f_E)^{5/2}]$ and $f_E = 1/2[(V_0/V)^{2/3} - 1]$, and Poirier–Tarantola EoS (**b**), $P_n = P/[3(V_0/V)f_N]$ and $f_N = 1/3\ln(V/V_0)$

Structural behaviour at high pressure

In spinels, the bond-length compressibility can be split into two components: one (β_a) is the cell-edge compressibility, whereas the other (β_u) depends on the first derivative of u versus P (Nakagiri et al. 1986). Our u values versus P appear scattered around their average and oscillate between 0.2555 and 0.2570. We fitted a linear function of P to the us, resulting in a slope of 1.4(7) 10^{-5} GPa^{-1}; the low level of significance of the slope ($\approx 2\sigma$) confirms a modest sensitivity of u to P. Therefore, the dependence of u on P is out of the resolution provided by the technique used here. Assuming $\partial u/\partial P \approx 1.4\ 10^{-5}$ GPa^{-1}, the term dependent on $\partial u/\partial P$ of the T–O bond length compressibility results in approximately 1.1 10^{-4} GPa^{-1}, against 1.84 10^{-3} GPa^{-1} [i.e. $1/(3\ K_0)$] due to β_a. A comparable value of β_u holds for the other bond length [M–O], also, in MgFe-spinel. In this view, β_a: β_u is some 18:1, which implies that most of the structure shrinking takes place at the expense of the lattice edge, and the strain affecting MgFe-spinel upon P is mainly of homogeneous nature. Such a conclusion is similar to that claimed by Levy et al. (2003), in the case of $MgAl_2O_4$.

Andrault and Bolfan–Casanova (2001) report a phase transition which spinel Mg-ferrite undergoes at about 20 GPa to a $CaMn_2O_4$-like structure, wherein Ca has eightfold coordination. The quoted authors observed the coexistence of two polymorphs of $MgFe_2O_4$ in the range from 18 to 27 GPa, which they attribute to a possible lack of pressure control upon laser heating, and/or to the occurrence of thermal gradients. In our experiment we did not observe hints of any phase transformation up to 35 GPa; neither was any anomalous behaviour of the polyhedral bond lengths revealed, which, on the contrary, took place in $ZnFe_2O_4$ as a prelude to a structural transition to a $CaMn_2O_4$-like structure at about 25 GPa (Levy et al. 2000). The discrepancies with Andrault and Bolfan–Casanova (2001) might be due to a slow reaction kinetics in our experiment, which was not assisted by a heating supply; such an aspect will be reconsidered in the Phase relation diagram calculations section below. However, the similarity between $MgFe_2O_4$ and $ZnFe_2O_4$ is misleading if restricted to a cation replacement only, as it involves a more substantial aspect, the former spinel having an inverse structure, the latter a normal one. In this view, the monotonic and regular shortening of the T–O and M–O bond lengths in Mg-ferrite, compared with the non-monotonic trend in Zn-ferrite, is presumably reflective of an intrinsic difference of the structural response to pressure of the two spinels. For $ZnFe_2O_4$, Levy et al. (2000) report: $K_0 = 166.4(\pm\ 3.0)$ GPa and $K' = 9.3(\pm\ 0.6)$. Furthermore, note that the Zn-coordinated tetrahedron in $ZnFe_2O_4$ results significantly softer than the Fe^{3+}– coordinated one in $MgFe_2O_4$, on account of both the bond lengths and the cation valences involved.

Order–disorder reaction as a function of temperature

The structural parameters of $MgFe_2O_4$ as a function of temperature are shown in Table 3; although the information in Table 3 is somewhat redundant to the ensuing discussion, it has been fully reported for the sake of completeness. The inversion parameter x corresponds to the fraction of Fe occupying the T site. x varies within 1 σ up to about 850 K (Fig. 4); at higher temperature it decreases, as the spinel tends to evolve towards a more disordered configuration [$x \rightarrow 2/3$]. At about 850 K, the cell parameter (a), which trends linearly as a function of T, shows a very slight change in slope (Fig. 5), consistent with the activation, at such a temperature, of the cation diffusion and reordering. Naturally, our in situ observation of a reordering at $T > 850$ K does not mean that the reaction has actually started at such a temperature; the onset might be at lower T, but unobservable by the present measurements because of a too slow kinetics. The modest change in the $a(T)$ curve can be neglected without a significant loss of precision, allowing us to treat the thermal expansion of $MgFe_2O_4$ by only one continuous function. Following Fei (1995), we have modelled the cell-edge thermal expansion coefficient by $\alpha_{a0} + \alpha_{a1}{}^*(T-298) + \alpha_{a2}/(T-298)^2$, obtaining $\alpha_{a0} =$ 9.1(1) 10^{-6} K^{-1}, $\alpha_{a1} = 4.9(2)\ 10^{-9}$ K^{-2} and $\alpha_{a2} = 5.1(5)$

Table 3 Results from structure Rietveld refinements under high-temperature conditions: lattice parameter (Å), u coordinate of oxygen, x order parameter, i.e. occupancy of Fe in the tetrahedral site, isotropic atomic displacement parameters (×100) for the tetrahedral site (U_T), octahedral site (U_M) and oxygen (U_O). R_{wp} sqrt[$\Sigma(I_o-I_c)^2 w$], where w = weighting factor. *Values in brackets* represent the standard error on the last decimal place

T(K)	a(Å)	x	u	U_T(Å^2)	U_M(Å^2)	U_O(Å^2)	R_{wp}
298	8.39389(5)	0.802(11)	0.2563(1)	1.98(9)	2.05(8)	2.3(1)	0.16
373	8.40154(7)	0.809(11)	0.2570(5)	2.01(9)	2.04(8)	2.2(1)	0.14
473	8.41250(7)	0.796(11)	0.2563(5)	2.37(10)	2.27(8)	2.6(1)	0.18
573	8.42373(7)	0.792(11)	0.2560(5)	2.45(10)	2.54(9)	2.8(2)	0.17
673	8.43323(7)	0.784(11)	0.2561(5)	2.58(11)	2.67(9)	2.8(2)	0.17
775	8.44207(7)	0.810(11)	0.2565(5)	2.74(11)	2.63(9)	2.7(2)	0.18
873	8.45200(7)	0.802(11)	0.2557(5)	2.69(11)	3.01(10)	3.4(2)	0.18
923	8.45600(7)	0.821(11)	0.2557(5)	2.67(11)	2.96(10)	3.2(2)	0.18
973	8.46280(7)	0.803(11)	0.2554(5)	2.98(11)	3.02(10)	3.4(2)	0.17
1023	8.46690(7)	0.796(11)	0.2560(5)	3.27(12)	3.27(10)	3.3(2)	0.19
1073	8.47260(7)	0.767(11)	0.2553(5)	3.39(12)	3.34(10)	3.8(2)	0.17
1123	8.47880(7)	0.755(11)	0.2556(5)	3.09(12)	3.26(10)	3.7(2)	0.19
1173	8.48400(6)	0.740(11)	0.2559(5)	3.30(12)	3.50(10)	3.8(2)	0.17
1223	8.48960(8)	0.747(13)	0.2557(6)	4.52(16)	4.33(12)	4.7(2)	0.19
1273	8.49630(7)	0.720(11)	0.2557(5)	3.82(13)	3.88(10)	4.4(2)	0.17
1323	8.50190(9)	0.727(12)	0.2562(6)	3.74(16)	4.34(14)	4.1(2)	0.19
1373	8.50749(6)	0.697(11)	0.2557(5)	3.82(14)	4.04(11)	4.3(2)	0.18
1473	8.52131(11)	0.694(13)	0.2555(7)	4.37(19)	5.02(16)	6.2(3)	0.19

10^{-2} K. Note that the bulk thermal expansion [$\alpha_V(T)$] is related to the cell-edge thermal expansion [$\alpha_a(T)$] as $\alpha_V(T) = 3\alpha_a(T)$.

The effect of the disorder reaction on the Gibbs energy may be estimated by taking into account that the inversion parameter is related to the lattice energy and to the configurational entropy through the thermodynamic model proposed by O'Neill and Navrotsky (1983, 1984):

$$\ln\left(\frac{x^2}{(1-x)(2-x)}\right) = -RT(\alpha + 2\beta x) \ ,$$

where α and β were derived by a weighting ($1/\sigma^2$) least-squares regression analysis of the experimental data; R is the universal gas constant ($R = 8.31$ J mol^{-1}). Using the results at $T > 850$ K, we obtain $\alpha = 22.2 \pm 1.8$ kJ mol^{-1} and $\beta = -17.6 \pm 1.2$ kJ mol^{-1}. A comparison with the issues by Kriessmann and Harrison (1956) and Epstein and Frankiewicz (1958), on the basis of saturation magnetisation measurements, reveals a good agreement between our results and those of the quoted authors (discrepancies on α and β confined within 6.2 and 1%, respectively). The α and β parameters from O'Neill et al. (1992), by X-ray powder diffraction on quenched samples, are 26.6 ± 0.4 kJ mol^{-1} and −21.7 ± 0.3 kJ mol^{-1}, respectively, yielding a discrepancy to ours of 18 ≈ 20%. However, such a deviation affects ΔU ($= \alpha\ x + \beta\ x^2$, contribution of the internal energy to the Gibbs energy, assuming the inverse structure as a reference) about 12–13%, as a consequence of a compensation between α and β. A ΔG ($= \Delta U - T\ \Delta S$, where the entropy is restricted to the configurational contribution) of about −5 kJ mol^{-1} follows from calculation, and results more than 20 times smaller than the ΔH between 300 and 900 K determined by integration of the specific heat with respect to temperature. This all suggests that the contribution to the

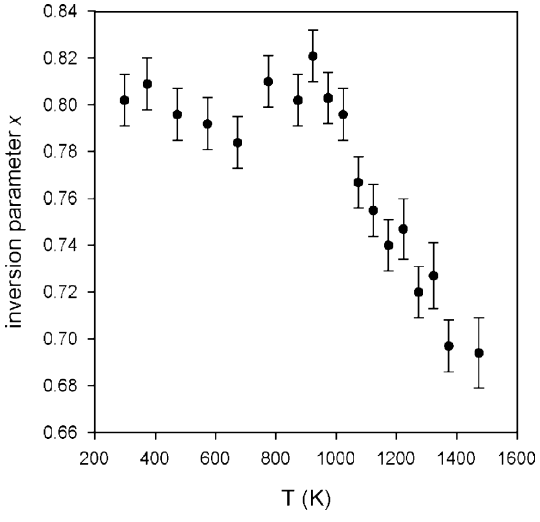

Fig. 4 Order parameter as a function of temperature

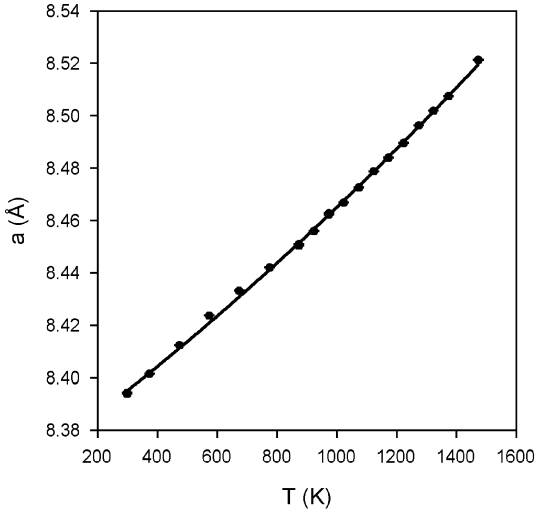

Fig. 5 Cell edge (Å) as a function of temperature (K). The *solid line* is the third order polynomial fit

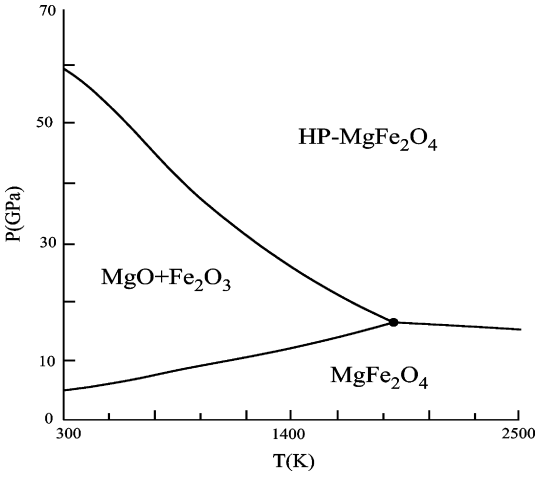

Fig. 6 Phase relation diagram of $MgFe_2O_4$ using the thermoelastic parameters here presented

Gibbs energy of the cation reordering is secondary in fixing the stability of $MgFe_2O_4$-spinel against that of the $CaMn_2O_4$-like phase or of the assemblage MgO + Fe_2O_3 under P–T conditions.

We have estimated the activation volume (ΔV) of the order-disorder reaction, as the difference between V measured at $T > 850$ K (i.e. above the "kink" in the volume versus temperature curve) and its value extrapolated by the $V(T)$ curve determined at lower temperatures. In so doing, we have obtained $\Delta V(\text{Å}^3) = 0.167$–$4.2751(x- < x >) + 112.7\ (x- < x >)^2$, where $< x > \approx 0.80$ is the average of x up to 775 K (Table 3). This proves that a cation rearrangement towards a more disordered structure (i.e. the same as effected by heating) leads to a less and less stable structure upon pressure, because of a $\Delta V > 0$.

Phase relation diagram calculations

In Figure 6 we report the phase diagram of $MgFe_2O_4$, calculated on the basis of (1) Mg-ferrite (data from the present work), (2) its high-pressure phase (data from Andrault and Bolfan–Casanova 2001) and (3) the constituent oxides (haematite and periclase; data from the database of Holland and Powell 1998). We have approximated H^f_{ref} of the high-pressure modification of $MgFe_2O_4$ by assuming it to exist at 17.7 GPa along with the spinel phase, following the results of Andrault and Casanova (2001). Moreover, we neglect the effect due to a possible cation re-arrangement in the spinel phase, because of the discussion reported in the Order–disorder reaction at high temperature section above. In so doing, we attain a phase diagram which predicts the spinel-like structure to decompose into haematite and periclase between 1.3 and 58 GPa at room temperature (see also Catti 2001, in the case of $MgAl_2O_4$), and to transform directly into the high-pressure phase of $MgFe_2O_4$ above 17 GPa, at $T > 1800$ K. Our observations did not reveal any reaction of decomposition up to 35 GPa and room temperature, most for likely kinetic reasons. Had we used the original themoelastic data of the database of Holland and Powell (1998) for Mg-ferrite, we would have observed an expansion of the stability field of the assemblage haematite + periclase, and predicted a transition spinel-to-high pressure phase at $T > 2300$ K.

Conclusions

Synthetic MgFe-spinel was investigated by in situ high-pressure powder diffraction and in situ high-temperature powder diffraction. The results obtained are summarised below:

1. The third-order Birch–Murnaghan EoS and Vinet EoS provide elastic parameters in full agreement, i.e. $K_0 = 181.5(\pm 1.3)$ GPa, $K' = 6.32(\pm 0.14)$ and $K'' = -0.0638$ GPa^{-1}.
2. The structure shrinks upon compression without significant change of the co-ordinate of oxygen. This implies occurrence of a homogeneous strain, similarly to the case for $MgAl_2O_4$.
3. Above 900 K, the cation-ordering reaction involving Fe and Mg over the tetrahedral and octahedral sites becomes apparent. However, given that the change of the curve of the lattice parameter as a function of temperature is negligible, one can describe the thermal expansion by a single function, i.e. $\alpha_{a0} + \alpha_{a1}{}^*(T-298) + \alpha_{a2}/(T-298)^2$, where $\alpha_{a0} = 9.1(1)\ 10^{-6}$ K^{-1}, $\alpha_{a1} = 4.9(2)\ 10^{-9}$ K^{-2} and $\alpha_{a2} = 5.1(5)\ 10^{-2}$ K.
4. The O'Neill model was fitted to the experimental data, and led to $\alpha = 22.2(\pm 1.8)$ kJ mol^{-1} and $\beta = -17.6(\pm 1.2)$ kJ mol^{-1}. Note that the role of the cation readjustment is a secondary contribution to the stability of MgFe-spinel against its $CaMn_2O_4$-like modifications or assemblage.
5. The phase diagram calculated using our thermoelastic results shows that below 1800 K MgFe-spinel decomposes upon pressure into the parent oxides, whereas it transforms into the high-pressure orthorombic phase at higher temperature. A comparison with the phase diagram predicted by using previous data for MgFe-spinel indicates that our results lead to an expansion of the $MgFe_2O_4$ phases at the expenses of haematite and periclase.

Acknowledgements The European Synchrotron Radiation Facility is kindly acknowledged. The National Research Council (CNR), Istituto per la Dinamica dei Processi Ambientali (IDPA), is acknowledged for the maintenance and functioning of the electron microprobe. The authors are grateful to Denis Andrault and Hans Annersten, who reviewed the manuscript and provided useful suggestions to improve it.

References

Akaogi M, Hamada Y, Suzuki T, Kobayashi M, Okada M (1999) High-pressure transition in the system $MgAl_2O_4$–$CaAl_2O_4$: a

new hexagonal aluminous phase with implication for the lower mantle. Phys Earth Planet Inter 115:67–77
Andrault D, Bolfan–Casanova N (2001) High-pressure phase transformations in the $MgFe_2O_4$ and Fe_2O_3–$MgSiO_3$ systems. Phys Chem Miner 28:211–217
Birch F (1986) Equation of state and thermodynamic parameters on NaCl to 300 kbar in the high-temperature domain. J Geophys Res 91:4949–4954
Catti M (2001) High-pressure stability, structure and compressibility of *Cmcm*-$Mg_2Al_2O_4$: an ab initio study. Phys Chem Miner 28:729–736
Connolly JAD (1990) Multivariable phase diagrams: an algorithm based on generalized thermodynamics. Am J Sci 290:666–718
Dapiaggi M, Artioli G, Petras L (2002) A newly developed high-temperature chamber for in-situ X-ray diffraction: setup and calibration procedures. Rigaku J 19:35–41
Duffy TS, Hemley RJ, Mao H (1995) Equation of state and shear strength at multimegabar pressures: magnesium oxide to 227 GPa. Phys Rev Lett 74:1371–1374
Epstein DJ, Frankiewicz B (1958) Some properties of quenched magnesium ferrites. J Appl Phy 29:376–377
Fei Y (1995) Thermal expansion. In: Ahrens TJ (ed) Mineral physics and crystallography: a handbook of physical constants. American Geophysical Union, Washington, DC, Reference Shelf 2
Fei Y, Frost DJ, Mao HK, Prewitt CT, Häusermann D (1999) In situ structure determination of the high-pressure phase of Fe_3O_4. Am Mineral 84:203–206
Finger LW, Hazen RM, Hofmeister AM (1986) High-pressure crystal chemistry of spinel ($MgAl_2O_4$) and magnetite (Fe_3O_4): comparison with silicate spinels. Phys Chem Miner 13:215–220
Funamori N, Jeanloz R, Nguyen H, Kavner A, Cadwell WA, Fujino K, Miyajima N, Shinmei T, Tomioka N (1998) High-pressure transformations in $MgAl_2O_4$. J Geophys Res 103:20813–20818
Hammersley AP, Svensson SO, Hanfland M, Fitch AN, Häusermann D (1996) Two-dimensional detector software: from real detector to idealised image or two-theta scan. High Pressure Res 14:235–248
Holland TJB, Powell R (1998) An internally consistent data set for phases of petrological interest. J Metamorph Geol 16:309–343
Irifune T, Fujino K, Ohtuni E (1991) A new high-pressure form of $MgAl_2O_4$. Nature 349:409–411
Kesson SE, Fitz Gerald JD, Shelley JMG (1994) Mineral chemistry and density of subducted basaltic crust at lower mantle pressures. Nature 372:767–769
Kriessmann CJ, Harrison SE (1956) Cation distributions in ferrospinels; magnesium-manganese ferrites. Phys Rev 103:857–860
Larson AC, Von Dreele RB (2000) General structure analysis system (GSAS). Los Alamos National Laboratory Report. LAUR: 86–748
Levy D, Pavese A, Hanfland M (2000) Phase transition of synthetic zinc ferrite spinel ($ZnFe_2O_4$) at high pressure, from synchrotron X-ray powder diffraction. Phys Chem Miner 27:638–644
Levy D, Pavese A, Hanfland M (2003) Synthetic $MgAl_2O_4$ (spinel) at high-pressure conditions (0.0001–30 GPa): an X-ray powder diffraction by synchrotron radiation. Am Mineral 88:93–98
Liu LG (1978) A new high-pressure phase of spinel. Earth Planet Sci Lett 41:398–404
Mao HK, Xu J, Bell PM (1986) Calibration of the ruby pressure gauge to 800 kbar under quasi-hydrostatic conditions. J Geophys Res 91:4673–4676
Nakagiri N, Manghnani MH, Ming LC, Kimura S (1986) Crystal structure of magnetite under pressure. Phys Chem Miner 13:238–244
Navrotsky A (1994) Physics and chemistry of Earth materials. Cambridge University Press, UK
O'Neill HStC, Navtrosky A (1983) Simple spinels: crystallographic parameters, cation radii, lattice energies and cation distributions. Am Mineral 68:181–194
O'Neill HStC, Navtrosky A (1984) Cation distribution and thermodynamic properties of binary spinel solid solutions. Am Mineral 69:733–753
O'Neill HStC, Annersten H, Virgo D (1992) The temperature dependence of the cation distribution in magnesioferrite $MgFe_2O_4$ from powder XRD structural refinement and Mössbauer spectroscopy. Am Mineral 77:725–740
Pavese A (2002) Pressure–volume–temperature equations of state: acomparative study based on numerical simulations. Phys Chem Miner 29:43–51
Pavese A, Artioli G, Hull S (1999) Cation partitioning versus pressure in $Mg_{0.94}Al_{2.04}O_4$ synthetic spinel, by in situ powder neutron diffraction. Am Mineral 84:905–912
Poirier JP, Tarantola A (1998) A logarithmic equation of state. Phys Earth Planet Inter 109:1–8
Redfern SAT (2002) Neutron powder diffraction of minerals at high pressures and temperatures: some recent technical developments and scientific applications. Eur J Mineral 14:251–261
Sack RO (1982) Spinels as petrogenetic indicators: activity composition relations at low pressures. Contrib Mineral Petrol 79:169–186
Singh AK (1993) The lattice strains in a specimen (cubic system) compressed non-hydrostatically in an opposed anvil device. J Appl Phys 73:4278–4286
Swenson CA (1983) Recommended values for the thermal expansivity of silicon from 0 to 1000 K. J Phys Chem Ref Data 12:179–182
Toby BH (2001) EXPGUI, a graphical user interface for GSAS. J Appl Crystallogr 34:210–213
Vinet P, Ferrante J, Smith JR, Rose JH (1986) A universal equation of state for solids. J Phys (C) Solid State 19:L467–L473
Vinet P, Smith JR, Ferrante J, Rose JH (1987) Temperature effects on the universal equation of state of solids. Phys Rev (B) 35:1945–1953
Wang ZW, Lazor P, Saxena SK, O'Neill HStC (2002) High pressure Raman spectroscopy of ferrite $MgFe_2O_4$. Mater Res Bull 37 (9):1589–1602

View publication stats